Accounting for magnetic saturation in designing a SRM speed controller for torque ripple minimization

Youness Boumaalif, Hamid Ouadi

Laboratory of Electrotechnics, Robotics and Automation (ERERA), National School of Arts and Crafts (ENSAM),
Mohammed V University, Rabat, Morocco

Article Info

ABSTRACT

This study established a nonlinear control design for switched reluctance motor (SRM) vehicle applications, using the backstepping approach. The suggested controller is established according to a model that consider magnetic saturation while reducing torque ripple and resulting in less vibrations. To optimize torque ripple, control angles are adjusted based on the machine speed and torque measurements. Indeed, a lookup table is constructed, offering the efficient control angles for various motor operating points. The suggested control technique was validated through simulation, exploiting an accurate MATLAB SRM model considering magnetic saturation effects. To illustrate the superiority of the suggested regulator, a comparison of its performance with a proportional-integral (PI) controller was performed. The acquired findings indicate the suggested regulator's effectiveness.

Corresponding Author:

Youness Boumaalif
Laboratory of Electrotechnics, Robotics and Automation (ERERA), National School of Arts and Crafts (EN-SAM), Mohammed V University
Rabat, Morocco
Email: boumaalif.youness@gmail.com

1. INTRODUCTION

Switched reluctance machines are distinguished from other electrical machines because their structure is devoid of conductors and magnets, which allows them to operate at different speeds. These machines also have other advantages, including simple and less expensive design, high torque production and so on [1]-[3]. But its nonlinear magnetic characteristic poses a number of challenges, including vibration, acoustic noise, and significant torque ripple [4].

In the literature, numerous studies on machine mechanical design have been established to decrease the torque ripple of swithed reluctance motor [5]-[8]. But this type of solution is expensive and presents practical implementation challenges [9]. Other studies have been conducted adopting control procedures, for instance, currents controllers , excitation angles optimization, and so on. In [10] an adaptive excitation angles optimization has been proposed. However, the magnetic saturation phenomena has not been considered in the control model development. For decades, many studies on machines and their controls have been developed considering linear regime[11]-[13]. The limitation to the linear regime, whether for the machines or the controllers, does not guarantee good performance. In [14]-[16], an advanced torque sharing function (TSF) has been established. However, this technique use an switched reluctance motor (SRM) model neglecting magnetic saturation, i.e., the expression of the inductance $L_j(\theta)$ (where j represents the considered phase number), was given according to the position only. Thus the performance of these regulators is only ensured for current

values lower than the nominal value. Therefore, the SRM must be decommissioned.

Masoudi *et al.* [17] suggested a fuzzy adaptive control method to decrease torque ripple. The chosen control model does not considere the magnetic saturation. Thus, the outcomes obtained are unsatisfactory. Besides, a speed control technique with torque ripple minimization has been given in [18], while acting on both current and control angles. Its main drawback is that the magnetic saturation effects are not taken into account when designing its algorithm. To increase the machine's performance, magnetic saturation effects should be considered, hence the expression of the inductance L_j should take into account both current i_j and rotor position θ (see Figure 1).
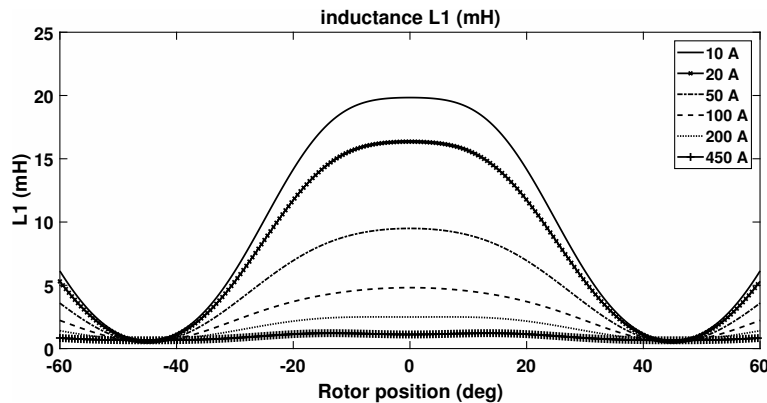

Figure 1. Inductance L_1 form

Many studies based on nonlinear control technique have been investigated taking into account the magnetic saturation. For instance, intelligent controller, sliding mode controller, predictive controllers, and so on. In comparison with [19], predictive control provides lower torque ripple. Because of the requirement to identify the target function future values, it requires massive computations [20]. Similarly, sliding mode control (SMC) considered in [21]-[23]. Nhan *et al.* [21] describes the design and study of SMC for radial position and rotational speed of slotless self-bearing motors. In [23], a control study of an induction motor powered by a solar photovoltaic (SPV), using a sliding mode controller and a hysteresis controller has been investigated. Applying this control technique to reduce torque ripple in an SRM is not allowed because to the chattering issue. Furthermore, Pushparajesh *et al.* [24] propose a direct torque scheme based on genetic neural network controllers to decrease the switched reluctance motor torque ripple. A drawback of that method is when compared to the set performance, the calculation time is a little higher. To improve the SRM performances, for example, wide speed range and supported large load torque. The controller design model should be carried out considering the magnetic saturation phenomena. Thus, the SRM machine modeling should be expressed in nonlinear form of position and current. Furthermore, we can act on both control angles (θ_{ON} and θ_{OFF}) and phase current. According to the aforementioned discussion, dealing with torque ripple minimization while considering the magentic saturation are still one of the most significant challenges in control fields. This motivates us to carry out this work. The major contribution of this study is to establish a new control technique including magnetic saturation effects in the purpose to improves SRM performances. This controller is intended to meet the following aims: (i) optimize the control angles in order to decrease torque ripple, (ii) track the desired speed, and (iii) track the desired torque.

Two nonlinear speed/current controllers are included in the proposed control approach using an optimal angles selection. Based on a model wish consider the magnetic saturation, nonlinear controllers are designed with the use of the backstepping approach. To reduce torque ripple, an excitation angles selection is carried out. The simulation outcomes are carried out using an SRM MATLAB model, that gives consideration to saturations effects. To prove the suggested approach efficiency, a comparison with proportional-integral (PI) controller is performed. The structure of this work is given as: switched motor modeling is depicted in section 2. Section 3 presents the design of the nonlinear controllers and the control angles selection. The simulation outcomes are developed in section 4. A conclusion is given at the end of this paper.

2.   SWITCHED RELUCTANCE MOTOR MODEL

As dicussed above, magnetic saturation should be considered when developing the SRM model, for the purpose of optimize motor performances. Thus, the current per phase and position must appear in the expression of the machine parameters. Using machine magnetic characteristic as shown in Figure 2, the phase inductance modeling is carried out as proposed in [25]. Based on electrical and dynamics fundamental formulas, we can elaborate these equations [10]:

$$
\begin{aligned}
\frac{di_1}{dt} &= -(\alpha_1 + \beta_1 \cdot \omega) \cdot i_1 + \gamma_1 \cdot u_1 \\
\frac{di_2}{dt} &= -(\alpha_2 + \beta_2 \cdot \omega) \cdot i_2 + \gamma_2 \cdot u_2 \\
\frac{di_3}{dt} &= -(\alpha_3 + \beta_3 \cdot \omega) \cdot i_3 + \gamma_3 \cdot u_3 \\
\frac{d\omega}{dt} &= -\frac{f}{\tilde{J}} \cdot \omega + \frac{1}{\tilde{J}} \cdot T_e - \frac{1}{\tilde{J}} \cdot T_L
\end{aligned}
\tag{1}
$$

with i_j represent the current per phase; u_j the control signal; T_e the instantaneous torque; θ the position; ω the speed; T_L the torque load; f the coefficient of the viscous friction ; and $\tilde{J}$ the inertia moment. The parameters α_j, β_j and γ_j are expressed as:

$$
\gamma_1 = \left(i_1 \cdot \frac{\partial L_1}{\partial i_1} + L_1 \right)^{-1} ; \alpha_1 = \gamma_1 \cdot R_1 ; \beta_1 = \gamma_1 \cdot \frac{\partial L_1 (\theta, i_1)}{\partial \theta}
$$

$$
\gamma_2 = \left(i_2 \cdot \frac{\partial L_2}{\partial i_2} + L_2 \right)^{-1} ; \alpha_2 = \gamma_2 \cdot R_2 ; \beta_2 = \gamma_2 \cdot \frac{\partial L_2 (\theta, i_2)}{\partial \theta}
$$

$$
\gamma_3 = \left(i_3 \cdot \frac{\partial L_3}{\partial i_3} + L_3 \right)^{-1} ; \alpha_3 = \gamma_3 \cdot R_3 ; \beta_3 = \gamma_3 \cdot \frac{\partial L_3 (\theta, i_3)}{\partial \theta}
$$

where R_j is the resistance per phase. Figures 3 and 4 show the general shape of $\frac{\partial L_j(\theta, i_j)}{\partial \theta}$ and $\frac{\partial L_j(\theta, i_j)}{\partial i_j}$ parameters, which are performed based on the modelisation proposed by [25].
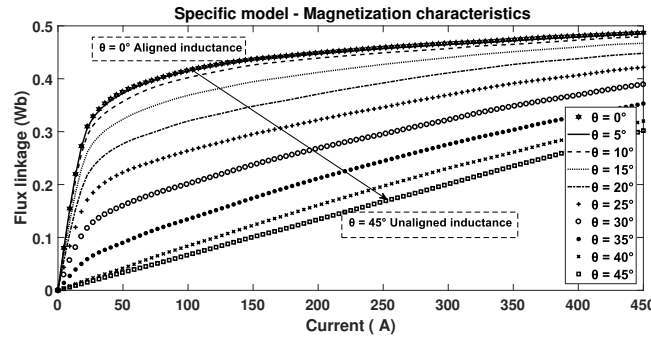

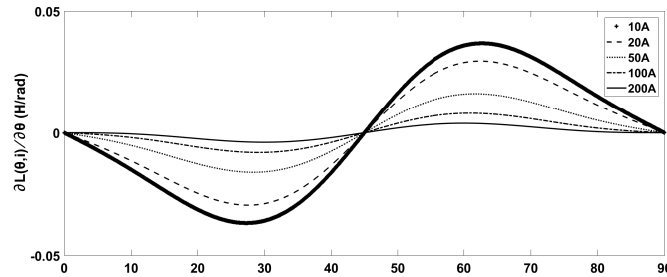Figure 2. SRM $\frac{6}{4}$ magnetic characteristics

Figure 3. The $\partial L_j(\theta, i_j)$ variation with respect to position
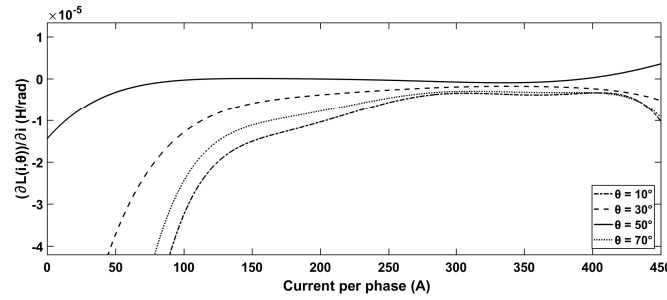
Figure 4. The $\partial L_j(\theta, i_j)$ variation with respect to phase current

Otherwise, the electromagnetic torque is given by [26]:

$$T_e = \sum_{j=1}^{N_{ph}} T_j \tag{2}$$

with:

$$T_j = \frac{\partial}{\partial \theta} \int_0^{i_j} \varphi(\tau, \theta) d\tau \tag{3}$$

where T_j is instantaneous torques per phase; $\varphi(\theta, i)$ the flux linkage and N_{ph} is the SRM phases number. If we choose $\overline{x}_1 = i_1$, $\overline{x}_2 = i_2$, $\overline{x}_3 = i_3$ and $\overline{x}_4 = \omega$ as state variable, the system of equation given by (1) becomes:

$$
\begin{aligned}
\dot{\overline{x}}_1 &= -(\alpha_1 + \beta_1 \cdot \overline{x}_4) \cdot \overline{x}_1 + \gamma_1 \cdot u_1 \\
\dot{\overline{x}}_2 &= -(\alpha_2 + \beta_2 \cdot \overline{x}_4) \cdot \overline{x}_2 + \gamma_2 \cdot u_2 \\
\dot{\overline{x}}_3 &= -(\alpha_3 + \beta_3 \cdot \overline{x}_4) \cdot \overline{x}_3 + \gamma_3 \cdot u_3 \\
\dot{\overline{x}}_4 &= -\frac{f}{\widetilde{J}} \cdot \overline{x}_4 + \frac{1}{\widetilde{J}} \cdot T_e - \frac{1}{\widetilde{J}} \cdot T_L
\end{aligned}
\tag{4}
$$

3. NONLINEAR CONTROLLERS DESIGN
3.1. Control approach

Instantaneous torque control (ITC) and average torque control (ATC) are the major SRM torque control techniques. When comparing these two methods, it can be shown that ATC has a significant torque ripple that might result in machine vibrations, which are not recommended in the industry [27]. The instantaneous torque control techniques is categorised as direct (DITC) or indirect (IITC). The IITC control the output torque by regulating phase current. In the literature, there are several categories of IITC approaches, including harmonic current injection, torque sharing functions (TSF), current profiling methods and so one [28]. In our study, TSF technique is addressed. Figure 5 illustrates the association of a TSF function with a speed controller required to produce the desired torque T_j^*. A torque-current lookup database is then associated to a second current controller so as to achieve the desired u_j. Furthermore, the θ_{ON} and θ_{OFF} angles are varied based on the SRM operating point.
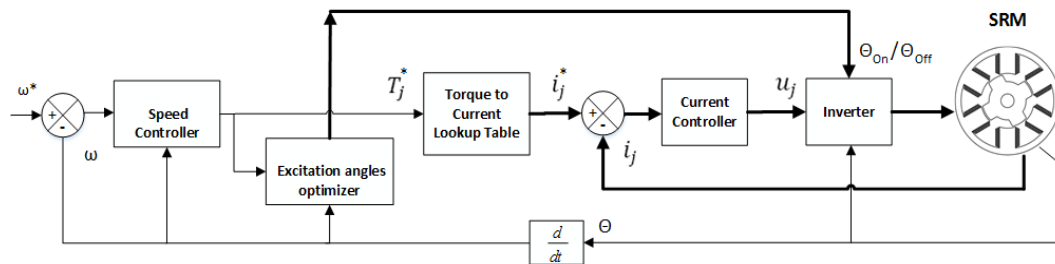

Figure 5. Proposed IITC controller

The suggested approach emphasizes two nonlinear backstepping controllers, a first table database for the desired current i_j^*, and a second one for the control angles optimization. For convenience, we recall that we attempt to meet the following control aims:

— Optimize the control angles to decrease torque ripple.
— Track the desired speed.
— Controlling the torque indirectly using currents.

3.2. Control angles selection

In the purpose to decrease the torque ripple, it is necessary to avoid the production of a negative torque. Therefore, the excitation angles(θ_{ON} and θ_{OFF}) should be chosen appropriately. In fact bad choice of these values, leads to apply a positif current throughout inductance negative changes ($\frac{\partial L}{\partial \theta} < 0$). Thus, it should be important to select θ_{ON} and θ_{OFF} such that they delimit the positive variation of the self-inductance (see Figure 6). As a result, good performance cannot be attained by a torque control with set control angles. This encourages the notion of modifying these angles based on the motor's operating point. Using an accurate MATLAB SRM 6/4 model, the optimal control angles were selected after several simulations. By computing the torque ripple ratio for distinct values of velocity and torque using the formula: $T_{ripple}(\%) = \frac{Te_{max} - Te_{min}}{T_a} \times 100\%$. Where Te_{max}, T_a, and Te_{min} are the higher, average and lower torque respectively.
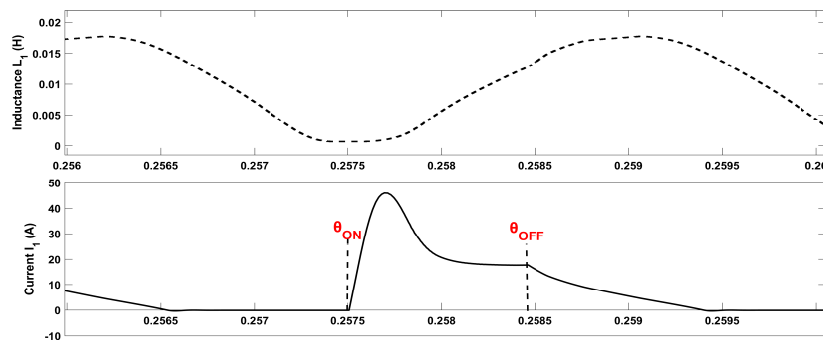

Figure 6. The application of a positive current during the interval θ_{ON} and θ_{OFF}

The T_{ripple} for every (ω, T_e) pair is computed for different values of excitation angles. Finally, we maintain the combination (θ_{ON} and θ_{OFF}) at a given torque and speed, ensuring the lowest torque ripple rate. Figure 7 illustrates an example of SRM torque ripple variation with respect to the excitation angles for a given torque T_e and speed ω (70 Nm and 200 rd/s). For this example, the optimal obtained pair is ($\theta_{ON} = 48°$, $\theta_{OFF} = 82.5°$). The entire collection of obtained measures is employed as lookup database that utilizes the speed and the instantaneous torque as inputs and θ_{ON}, θ_{OFF} as outputs.
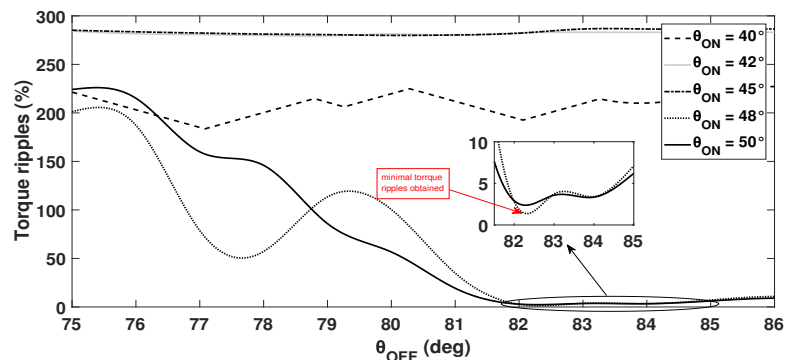

Figure 7. Torque ripple changes with θ_{ON} and θ_{OFF} for a fixed torque value $T_e = 70Nm$ and speed $\omega = 200 rad/s$

3.3. Design of the nonlinear controllers

3.3.1. Speed controller

The velocity controller is designed utilizing the backstepping method. Let define the velocity error:

$$\bar{e}_1 = \bar{x}_4 - \omega^* \tag{5}$$

where ω^* is the desired speed. The candidate Lyapunov function under consideration is presented as:

$$\bar{V}_1 = \frac{1}{2}\bar{e}_1^2. \tag{6}$$

Its time derivative is obtained by using (4) and (5) as:

$$\dot{\bar{V}}_1 = \bar{e}_1 \cdot \dot{\bar{e}}_1 = \bar{e}_1 \cdot \left(-\frac{f}{\tilde{J}} \cdot \bar{x}_4 + \frac{1}{\tilde{J}} \cdot T_e - \frac{1}{\tilde{J}} \cdot T_L - \dot{\omega}^* \right) \tag{7}$$

Let consider T_e as a virtual command, such that:

$$T_e = -\tilde{J} \cdot l_1 \cdot \bar{e}_1 + f \cdot \bar{x}_4 + \tilde{J} \cdot \dot{\omega}^* + T_L \tag{8}$$

where $l_1 > 0$ is a controller parameter. In this situation, one has:

$$\dot{\bar{V}}_1 = -l_1 \cdot \bar{e}_1^2 < 0 \tag{9}$$

as a result, the velocity error $\bar{e}_1$ is globally, asymptotically stable. On the other hand, T_e doesn't represent a real control input, so should not be immediately applied in accordance with (7). Thus, we designate the torque reference signal by T_e^*:

$$T_e^* = -\tilde{J} \cdot l_1 \cdot \bar{e}_1 + f \cdot \bar{x}_4 + \tilde{J} \cdot \dot{\omega}^* + T_L \tag{10}$$

the next objective is to ensure that T_e pursues its reference $T_e{}^*$.

3.3.2. Torque-current table

It should be noted that the currents per phase i_j^* are generated using the association of TSF block with torque-current database (view Figure 5). A adapted TSF function is employed in this paper. It has recently been established in [29] that this function provides the best solution for reducing torque ripple. Accordingly, $TSF(\theta)$ function is given by:

$$\text{TSF}(\theta) = \begin{cases} 0, & (0 \leq \theta \leq \theta_{on}) \\ \frac{T_e^*}{2} - \frac{T_e^*}{2}\cos\frac{\Pi}{\theta_{ov}}\left(\theta - \theta_{on}\right), & (\theta_{on} \leq \theta \leq \theta_{on} + \theta_{ov}) \\ T_e^*, & (\theta_{on} + \theta_{ov} \leq \theta \leq \theta_{off}) \\ \frac{T_e^*}{2} + \frac{T_e^*}{2}\cos\frac{\Pi}{\theta_{ov}}\left(\theta - \theta_{off}\right), & (\theta_{off} \leq \theta \leq \theta_{off} + \theta_{ov}) \\ 0, & (\theta_{off} + \theta_{ov} \leq \theta \leq \theta_p) \end{cases} \tag{11}$$

with θ_p, θ_{ov} are rotor period and overlap angle respectively. Based on (3) and the SRM 6/4 magnetic characteristic, a torque-current lookup table is constructed. Moreover, an inverse lookup table $i_j^*(T_j, \theta)$ is created by exploiting an interpolation function [29]. Now that the reference currents are determined, one can develop the second controller.

3.3.3. Current controller

Let consider the current errors given by:

$$\bar{z}_j = \bar{x}_j - i_j^*, \quad j = 1, 2, 3 \tag{12}$$

for the current errors system $\bar{z}_j$, the chosen Lyapunov candidate function is given by (13).

$$\bar{V}_2 = \sum_j \frac{1}{2}\bar{z}_j^2 = \frac{1}{2}\left(\bar{z}_1^2 + \bar{z}_2^2 + \bar{z}_3^2\right) \tag{13}$$

Using (4) and (12), one can obtain:

$$\dot{V}2 = \sum_j \left[\bar{z}_j \cdot \left(-\alpha_j \cdot \overline{x}_j - \beta_j \cdot \overline{x}_j \cdot \overline{x}_4 + \gamma_j \cdot u_j - \dot{i}_j^* \right) \right] \tag{14}$$

by using (14), the chosen control inputs are:

$$u_j = (\alpha_j)^{-1} \cdot \left(-k_j \bar{z}_j + \dot{i}_j^* + \alpha_j \cdot \overline{x}_j + \beta_j \cdot \overline{x}_j \cdot \overline{x}_4 \right) \tag{15}$$

where $k_j > 0$ are the controller parameters. By swapping (15) for (14), one has:

$$\dot{V}_2 = -\sum_j k_j \cdot \bar{z}_j^2 < 0 \tag{16}$$

as a result, the current regulator's error $\bar{z}_j$ is globally and asymptotically stable. The following theorem sums up the results of this analysis:

Theorem 3..1 (main result) considering the closed-loop system which consists of an SRM model, given by the dynamic system (1)-(4), and a nonlinear regulator provided by (15). Consequently, the ensuing properties are assured:

− The error system of currents ($\bar{z}_1$, $\bar{z}_2$, $\bar{z}_3$) has a global and asymptotic convergence to zero.

− Also, the error of torque $\bar{e}_1$ has a global and asymptotic convergence to zero.

Proof 1 the first section is proved by (16). Therefore each current i_j track its reference i_j^* in steady state. Furthermore, to enforce the motor torque to track its reference T_e^* given by (10), the currents per phase i_j^* were obtained based on the association of TSF function (11) with a lookup table. As a result, the SRM torque T_e will track its reference T_e^*. This concludes the proof of the second section of the theorem.

4. RESULTS AND DISCUSSION

To confirm the suggested control method superiority, simulations were performed using an SRM 6/4 MATLAB model while considering saturation. The major characteristics of the used motor are presented in the Tables 1 and 2. Indeed, a Simulink MATLAB model of the considered system is shown in Figure 8. A backstepping controller is used to achieve the speed tracking objective. This latter gives rise to the motor torque reference signal. A TSF function is then applied to determine the torque reference associated with each motor phase. Finally, using a lookup table, the desired torque is converted into corresponding current reference signal. The current controller drives the power converter associated to the SRM motor. Furthermore, an optimization unit is introduced for the adaptation of the converter control angles according to the SRM operating point. In this section, a performance comparison of the suggested controller with a PI regulator is carried out. Moreover, the consequences of varying θ_{ON} and θ_{OFF} is investigated. Lastly, the suggested controller's strength to load torque changes is assessed.

Table 1. SRM 6/4 characteristics

Parameters	Value
Stator and rotor poles	$\frac{6}{4}$
Phases number	3
Maximum power	60 kW
Phase voltage	240 V
Resistance per phase	0.05 Ω
Max current per phase	450 A
Max flux linkage per phase	486 mWb
Rotor friction	0.01 $N.m.s$
Rotor inertia	82.10^{-4} $Kg.m^2$
Saturated aligned inductance	$0.15.10^{-3}$ H
Aligned inductance	$23.6.10^{-3}$ H
Unaligned inductance	$0.67.10^{-3}$ H

Table 2. Considered parameters

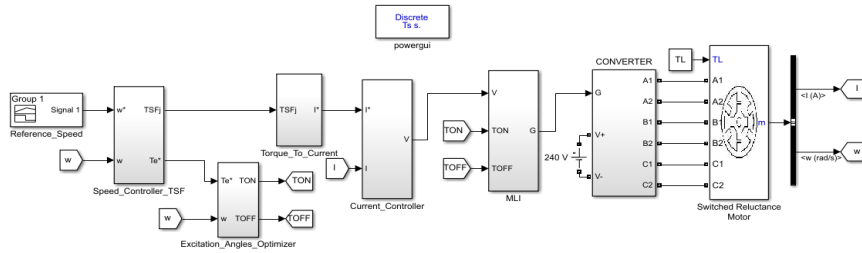| Parameters	Values
Standard PI	$\bar{K}_I = 150$
$\bar{K}_p = 1$	
Suggested controller	$k_1 = 24.10^4$
$k_2 = 24.10^4$	
$k_3 = 24.10^4$	
$l_1 = 10^5$	
Constants excitation angles	$\theta_{ON} = 48°$
$\theta_{OFF} = 80°$	

Figure 8. Simulink circuit scheme

4.1. Comparison of PI with the suggested controller

Based on control law provided by (10)-(15) when applied to the SRM 6/4 MATLAB model, the comparison is carried out. Figure 9 shows the speed responses of the two controllers when the speed takes 100 and 200 rad/s respectively with $T_L = 30 Nm$. It can be seen clearly the appearance of a overshoot due to PI regulator requiring more time to stabilize. In contrast, the two regulators perfectly follow the speed reference. Figure 10 illustrates the torque forms obtained with these two regulators. It is obvious that the suggested regulator minimizes T_{ripple} significantly, which proves its efficiency. Figure 11 depicts the phase voltage V_1 when the phase current track its reference. Moreover, Table 3 illustrates this comparison.
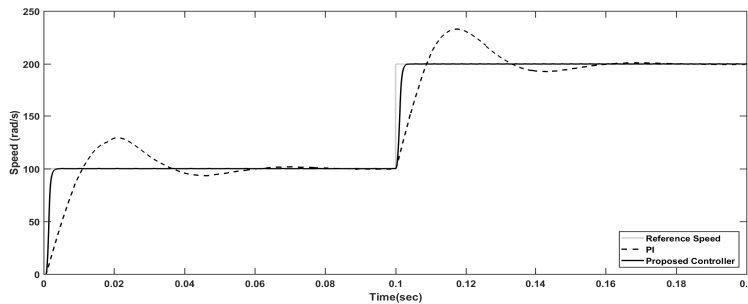
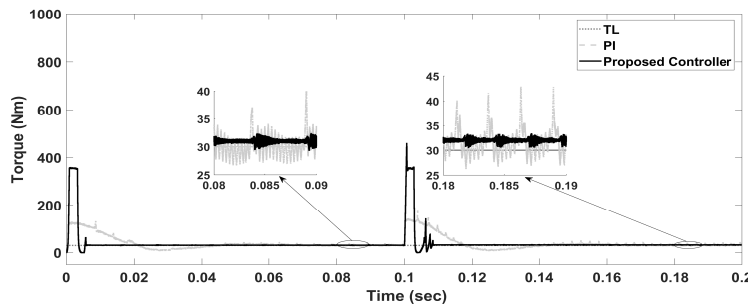Figure 9. The speed shape of the two controllers

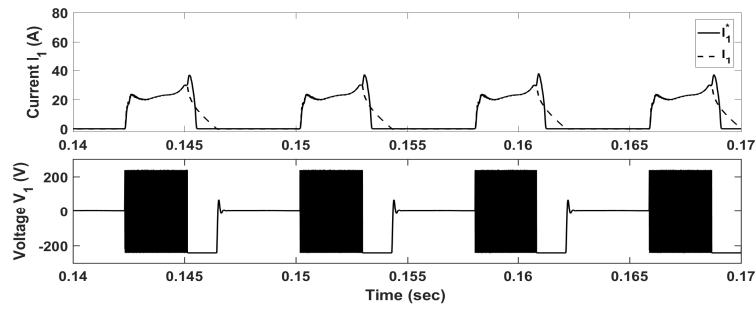Figure 10. The torque shape of the two controllers

Figure 11. Responses of the phase voltage V_1 and current per phase I_1

Table 3. A comparison of speed and torque ripple of both controllers

$\omega^*(rad/sec)$	Velocity error (rad/sec)		T Ripple $(\%)$	
	P.I	Suggested regulator	P.I	Suggested regulator
100	0.7	10^{-4}	45.28	8.95
200	0.4	3.10^{-3}	52.37	9.63

4.2. Influence of control angles

To demonstrate the advantage of modulating the θ_{ON} and θ_{OFF} parameters, a comparison of the proposed controller performances (for fixed and variable excitation angles) is performed. Figures 12 and 13 depicts the phase current, torque, and speed forms for fixed and modified control angles with a fixed load torque of 150 Nm. We can observe that the velocity response still follows its setpoint with minimal torque ripple. Table 4 highlight this comparison. Figure 14 shows the variation of excitation angles when applying a reference speed of 100 rad/s for t ranging from zero to 0.1 s and 200 rad/s for t from 0.1 to 0.2 s with a torque load of 150 Nm. We can see that our controller provides the optimal doublet $(\theta_{ON}, \theta_{OFF})$ which ensures the required performance based on desired speed and torque.
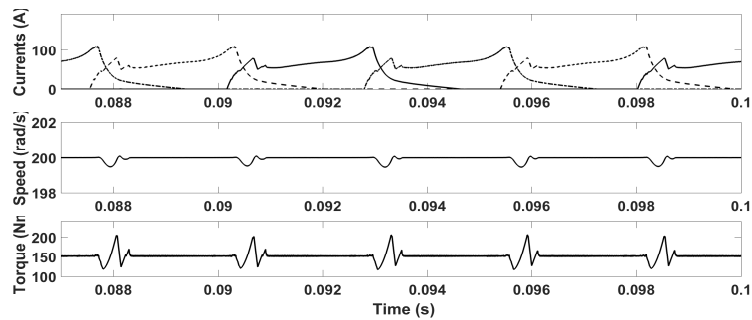

Figure 12. Responses of currents, velocity and torque with constants $\theta_{ON}, \theta_{OFF}$
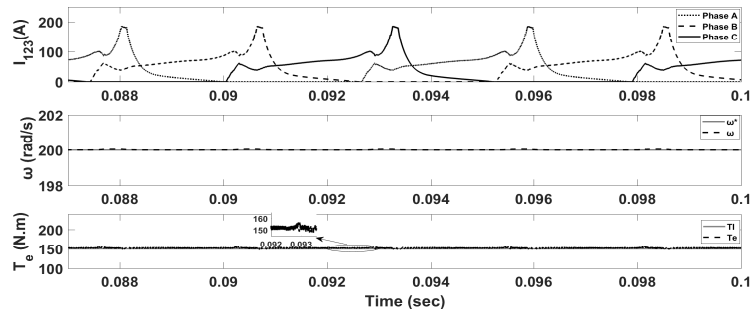

Figure 13. The currents, speed and torque shapes with controlled angles $(\theta_{ON}, \theta_{OFF})$

Table 4. A performances comparison for constants and adapted $(\theta_{ON}, \theta_{OFF})$

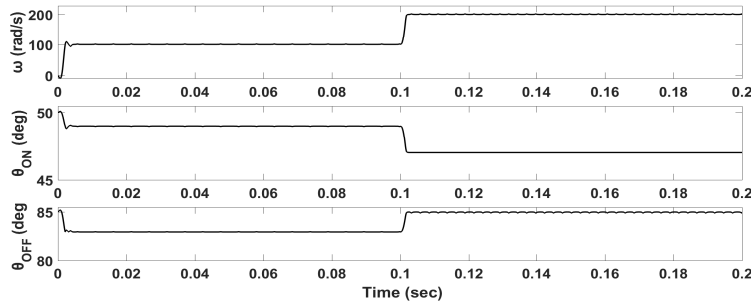|	Velocity error (rad/s)	T ripple (%)
Constants angles	0.59	66.3
Adapted angles	$0.42.10^{-3}$	6.33

Figure 14. Excitation angles $(\theta_{ON}, \theta_{OFF})$ shapes for a variable reference speed

4.3. Proposed controller robustness

To highlight the suggested regulator robustness, a varying resistant couple. with fixed speed (200 rad/s) is applied. Figures 15 and 16 show the shapes of speed and torque with variable load torque. It is clear that, regardless of load torque fluctuations, the proposed controller guarantees a speed tracking towards its reference with minimal torque ripple. Despite high torque value, the simulation outcomes prove the velocity regulation efficiency of the proposed controller as well as a minimization of torque ripple. Moreover, its immunity to load torque fluctuations has been demonstrated.
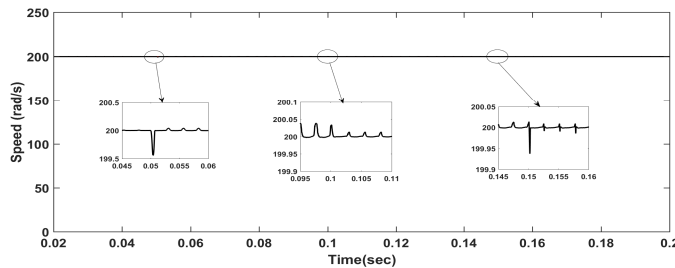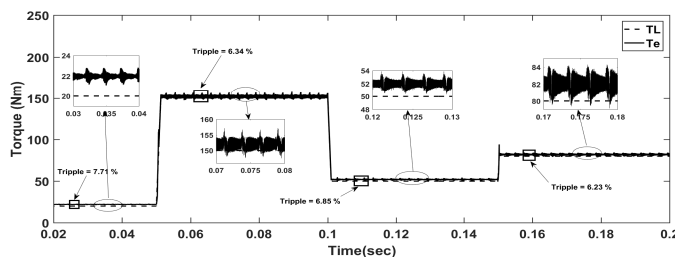

Figure 15. Speed form for variable load

Figure 16. Torque form for variable load (20, 150, 50 and 80 Nm successively)

5. CONCLUSION

This work designed a backstepping SRM controller while giving consideration to magnetic saturation effects and guarantying a torque ripple minimization. To more enhance the performance requirements, particularly, particularly when the load torque increases, an optimum excitation angles lookup-table has been used. Based on a Simulink model, considering magnetic saturation effects, the simulation has been carried out. The

outcomes demonstrate that the suggested regulator greatly reduces the T_{ripple} compared to the standard PI. Further, the velocity tracking error is less than $10^{-3}\ rad/s$. Furthermore, it has been illustrated that, as compared to fixed control angles, the employment of adaptive excitation angles improves machine performance. Finally, the suggested controller's robustness test has been accomplished.

REFERENCES
[1] I. Boldea, "Electric generators and motors: an overview," in *CES Transactions on Electrical Machines and Systems*, vol. 1, no. 1, pp. 3–14, 2017, doi:/10.23919/tems.2017.7911104.
[2] E. Bostanci, M. Moallem, A. Parsapour, and B. Fahimi, "Opportunities and challenges of switched reluctance motor drives for electric propulsion: a comparative study," in *IEEE Transactions on Transportation Electrification*, vol. 3, no 1, pp. 58-75, 2017, doi: 10.1109/TTE.2017.2649883.
[3] K. Kiyota, T. Kakishima, A. Chiba, and M. A. Rahman, "Cylindrical rotor design for acoustic noise and windage loss reduction in switched reluctance motor for HEV applications," in *IEEE Transactions on Industry Applications*, vol. 52, no. 1, pp. 154-162, 2016, doi: 10.1109/TIA.2015.2466558.
[4] S. M. Castano, B. Bilgin, E. Fairall, and A. Emadi, "Acoustic noise analysis of a high-speed high-power switched reluctance machine: frame effects," *IEEE Transactions on Energy Conversion*, vol. 31, no. 1, pp. 69-77, Mar. 2016, doi: 10.1109/TEC.2015.2470079.
[5] N. Mekala and C. Muniraj, "Implementation of PI controller for 4f SRM drive using TMS320F28335," *International Journal of Power Electronics and Drive Systems (IJPEDS)*, vol. 5, no 3, pp. 283-292, 2015.
[6] C. Maheswari, R. Thottungal, and A. C.Divya, "A modified bridgeless converter for SRM drive with reduced ripple current," *International Journal of Power Electronics and Drive System (IJPEDS)*, vol. 6, no 2, pp. 362-369, 2015.
[7] A. Chiba *et al.*, "Torque density and efficiency improvements of a switched reluctance motor without rare-earth material for hybrid vehicles," in *IEEE Transactions on Industry Applications*, vol. 47, no. 3, pp. 1240-1246, 2011, doi: 10.1109/TIA.2011.2125770.
[8] K. Kiyota and A. Chiba, "Design of switched reluctance motor competitive to 60-kW IPMSM in third-generation hybrid electric vehicle," in *IEEE Transactions on Industry Applications*, vol. 48, no. 6, pp. 2303-2309, 2012, doi: 10.1109/TIA.2012.2227091.
[9] C. Gan, J. Wu, Q. Sun, W. Kong, H. Li, and Y. Hu, "A review on machine topologies and control techniques for low-noise switched reluctance motors in electric vehicle applications," in *IEEE Access*, vol. 6, pp. 31430-31443, 2018, doi: 10.1109/ACCESS.2018.2837111.
[10] M. Hamouda and L. Számel , "Optimum excitation angles for switched reluctance motor drives," in *XXXIII. Kando Conference*, pp. 128-142, 2017.
[11] N. H. Quang, N. P. Quang, D. T. Hai, and N. N. Hien, "On tracking control problem for polysolenoid motor model predictive approach," *International Journal of Electrical and Computer Engineering (IJECE)*, vol. 10, no 1, pp. 849-855, 2020, doi: 10.11591/ijece.v10i1.pp849-855.
[12] H. Ouadi, F. Giri, A. Elfadili, and L. Dugard, "Induction machine speed control with flux optimization," *Control Engineering Practice*, vol. 18, no 1, pp. 55-66, 2010, doi: 10.1016/j.conengprac.2009.08.006.
[13] N. C. Lenin and R. Arumugam, "Design and experimental verification of linear switched reluctance motor with skewed poles," *International Journal of Power Electronics and Drive Systems (IJPEDS)*, vol. 6, no 1, pp. 18-25, 2015.
[14] A. Rajendran and S. Padma, "H_∞ robust control technique for controlling the speed of switched reluctance motor," *Frontiers of Electrical and Electronic Engineering*, vol. 7, pp. 337-346, 2012, doi: 10.1007/s11460-012-0204-0.
[15] Y. Wei, M. Qishuang, Z. Poming, and G. Yangyang, "Torque ripple reduction in switched reluctance motor using a novel torque sharing function," *2016 IEEE International Conference on Aircraft Utility Systems (AUS)*, 2016, pp. 177-182, doi: 10.1109/AUS.2016.7748043.
[16] M. Dowlatshahi and M. Daryanush, "A novel modified turn-on angle control scheme for torque-ripple reduction in switched reluctance motor," *International Journal of Power Electronics and Drive Systems (IJPEDS)*, vol. 7, no 4, pp. 1110-1124, Dec. 2016, doi: 10.11591/ijpeds.v7i4.pp1110-1124.
[17] S. Masoudi, M. R. Soltanpour, and H. Abdollahi, "Adaptive fuzzy control method for a linear switched reluctance motor," *IET Electric Power Applications*, vol. 12, no. 9, pp. 1328-1336, 2018, doi: 10.1049/iet-epa.2018.0059.
[18] N. Saha and S. Panda, "Speed control with torque ripple reduction of switched reluctance motor by hybrid many optimizing Liaison gravitational search technique," *Engineering Science and Technology, an International Journal*, vol. 20, no 3, pp. 909-921, 2017, doi: 10.1016/j.jestch.2016.11.018.
[19] S. Mehta, M. A. Kabir, and I. Husain, "Extended speed current profiling algorithm for low torque ripple SRM using model predictive control," *2018 IEEE Energy Conversion Congress and Exposition (ECCE)*, 2018, pp. 4558-4563, doi: 10.1109/ECCE.2018.8558169.
[20] S. Kandhasamy, "Machine learning based SRM control using FPGAs for torque ripple minimization," *2020 International Conference on Artificial Intelligence in Information and Communication (ICAIIC)*, 2020, pp. 675-680, doi: 10.1109/ICAIIC48513.2020.9065241.
[21] V. D. Nhan, N. X. Bien, N. Q. Dich, and V. T. Ha, "Sliding-mode control design of a slotless self-bearing motor," *Bulletin of Electrical Engineering and Informatics*,vol. 11, no. 3, pp. 1297-1307, 2022, doi: 10.11591/eei.v11i3.3687.
[22] F. B. Salem, I. Bahri, H. Maamri, and N. Derbel, "A second-order sliding mode control of switched reluctance motor," *Electric Power Components and Systems*, vol. 48, no. 6-7, pp. 640-651, Aug. 2020, doi: 10.1080/15325008.2020.1797937.

[23] R. Pazhanimurugan, R. Bensraj, and C. R. Balamurugan, "Dynamic response investigation of PV based CLCIS fed IMD applications using HC and SMC," *Bulletin of Electrical Engineering and Informatics*, vol. 11, no 2, pp. 691-701, 2022, doi: 10.11591/eei.v11i2.3394.

[24] V. Pushparajesh, B. M. Nandish, and H. B. Marulasiddappa, "Hybrid intelligent controller based torque ripple minimization in switched reluctance motor drive," *Bulletin of Electrical Engineering and Informatics*, vol. 10, no. 3, pp. 1193-1203, 2021, doi: 10.11591/eei.v10i3.3039.

[25] A. Naitali, A. Aamoud, and A. Hammouch, "Grey-box modelling and parameter estimation of switched reluctance motors," *2014 IEEE Conference on Control Applications (CCA)*, 2014, pp. 352-357, doi: 10.1109/CCA.2014.6981371.

[26] H. E. Chakir, H. Ouadi, and F. Giri, "Managing a hybrid energy smart grid with a renewable energy source," *Asian Journal of Control*, vol. 21, no. 4, pp. 2060-2073, 2019, doi: 10.1002/asjc.1995.

[27] H. Hannoun, M. Hilairet, and C. Marchand, "Comparison of instantaneous and average torque control for a switched reluctance motor," *2008 IEEE International Symposium on Industrial Electronics*, 2008, pp. 675-680, doi: 10.1109/ISIE.2008.4677059.

[28] G. Fang, F. P. Scalcon, D. Xiao, R. P. Vieira, H. A. Gründling, and A. Emadi, "Advanced control of switched reluctance motors (SRMs): a review on current regulation, torque control and vibration suppression," in *IEEE Open Journal of the Industrial Electronics Society*, vol. 2, pp. 280-301, 2021, doi: 10.1109/OJIES.2021.3076807.

[29] M. V. de Paula, T. de Almada Lopes, T. A. dos Santos Barros, P. S. N. Filho, and E. R. Filho, "Mathematical modeling of switched reluctance machines: development and application," *Modelling and Control of Switched Reluctance Machines*, pp. 191-220, 2020, doi: 10.5772/intechopen.89061.

BIOGRAPHIES OF AUTHORS

Youness Boumaalif 🔘 📑 🆂🅲 ⟳ received the M.S. degree in electrical engineering from ENSAM Mohammed V University in 2018. He is actively pursuing a Ph.D. in Automatic Control engineering at ENSAM, Mohammed V University, Rabat, Morocco. His research focuses on nonlinear controllers. He can be contacted at email: boumaalif.youness@gmail.com.

Hamid Ouadi 🔘 📑 🆂🅲 ⟳ is a Professor at ENSAM School, Mohammed V University, Rabat, Morocco. His research focuses on control and modeling of electrical systems, enhancement of power quality, and incorporation of renewable energy. He can be contacted at email: hamidouadi3@yahoo.fr.